Electronic Supplementary Material (ESI) for Physical Chemistry Chemical Physics.

Electronic Supporting Information

Triplet-sensitized photon upconversion in deep eutectic solvents

Yoichi Murakami,*[a] Sudhir Kumar Das,*[a,b] Yuki Himuro,[a†] and Satoshi Maeda[a]

[a] *School of Engineering, Tokyo Institute of Technology, 2-12-1-I1-15 Ookayama, Meguro-ku, Tokyo 152-8552, Japan.*

[b] *Department of Chemistry, Raghunathpur College, Raghunathpur, Dist.-Purulia, West Bengal, Pin-723133, India.*

† Present affiliation: Isuzu Motors Limited

Solubilities of DPA in some representative DESs:

Table S1 Solubilities of DPA in some representative DESs at room temperature.

Type of DES[a]	**Solubility of DPA [M]**
$N_{4444}Cl\text{-}G_{1:4}$	4.8×10^{-4}
$ChCl\text{-}G_{1:2}$	Not soluble
$ChCl\text{-}EG_{1:2}$	2×10^{-5}

[a] G: Glycerol; EG: Ethylene Glycol; ChCl: Choline Chloride. See the main text for the naming rule of DESs.

During our initial preliminary trials to prepare samples using representative (i.e., hydrophilic) DESs, we carried out several quick checks of the solubilities of DPA in such DESs. It was found that the solubilities were generally low, i.e., typically less than 10^{-3} M. Table S1 shows some solubility values that we had recorded at that time. The chemicals used in these measurements were purchased from Sigma Aldrich (glycerol and ethylene glycol) and TCI (choline chloride). All the materials were dried before use following the procedure described in the Experimental section of the main text. After the formation of the DESs, they were further dried in our glovebox (where oxygen and moisture were kept below 1 ppm; see the Experimental section) to avoid possible absorption of moisture. In the measurement procedure, first, excess DPA powder was added to a DES (ca. 400 μL) in a glass vial. Then, the mixture was stirred in the glovebox for 1 h at 70 °C on a hotplate stirrer, and then at room temperature for additional 20 h or more to allow it to reach solubility equilibrium. Subsequently, the mixture was left to stand in the glovebox at room temperature for a few days. The resultant mixture looked opaque because of clouding caused by a fine solid of DPA that precipitated in the liquid. The mixture was filtered through a PTFE membrane filter (Merck-Millipore, Millex-SLLGC13NL; pore size: 0.2 μm) to obtain only the liquid phase, which was transparent and colorless without light scattering. The liquid was diluted with methanol and its UV-vis absorption spectrum was measured to determine the solubility of DPA in the DES.

Solubilities of DPA in the hydrophobic DESs used in this study:

The solubilities of DPA in the hydrophobic DESs employed in this study were one order of magnitude higher, as summarized in Table S2 below, than those in the typical hydrophilic DESs listed in Table S1. These solubilities ($>5 \times 10^{-3}$ M) were sufficient for the purpose of the present study. The solubility measurements were performed in the same manner as described above.

Table S2 Solubilities of DPA in the DESs used in the present study at room temperature.

Type of DES[a]	**Solubility of DPA [M]**
$N_{4444}Cl\text{-}DA_{1:3}$ (for sample #1)	7.2×10^{-3}
$N_{4444}Cl\text{-}DA_{1:2}$ (for sample #2)	7.7×10^{-3}
$N_{4444}Cl\text{-}DA_{1:1.5}$ (for sample #3)	7.6×10^{-3}
$N_{4444}Cl\text{-}DA_{1:1}$ (for sample #4)	9.4×10^{-3}
$N_{8888}Cl\text{-}DA_{1:2}$ (for sample #5)	6.5×10^{-3}

[a] See the main text for details of the DES notation.

Optical absorption spectra of the DESs used in this study:

The optical absorption spectra of the DESs used in this study were measured using quartz cuvettes with a 1-mm optical path length. The results are shown in Fig. S1 below. All the DESs were transparent and colorless in the visible region (>400 nm).

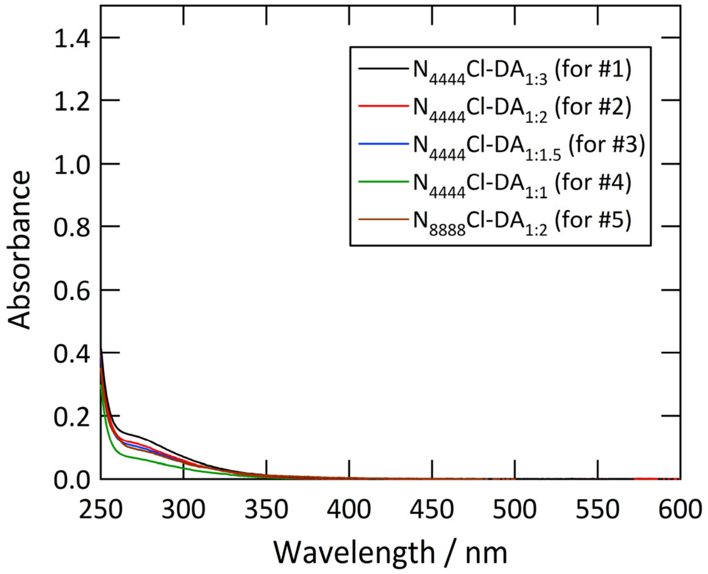

Fig. S1 UV-vis optical absorption spectra of the DESs. The optical path length was 1 mm.

Solvatochromic absorption peak shifts of PtOEP caused by the DESs:

The optical absorption peaks of PtOEP in samples #1–#5 are compared in Fig. S2 below. The results show that the solvatochromic shifts between the spectra are rather small (less than 1 nm).

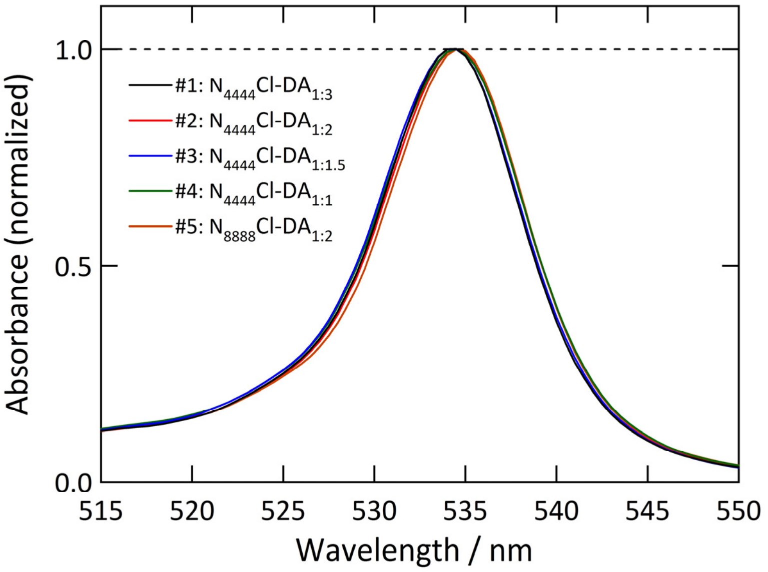

Fig. S2 Dependence of the optical absorption spectrum of PtOEP on DES measured for the sample #1–#5. The optical path length was 1 mm.

Summary of analytical methods (brief restatements of previously used methods):

All the analytical methods used in this article are the same as those previously employed, as cited accordingly below. They are briefly restated below using the symbols used in this article.

Determination of Φ_{UC}: Φ_{UC} was determined by a standard reference method.[S2,S3] The reference was a dye solution whose fluorescence quantum yield Φ_{R} was known. As described in the main text, we used a dilute toluene solution (2×10^{-5} M) of 9,10-bis(phenylethynyl)anthracene (BPEA) as the reference, whose Φ_{R} was reported to be almost unity.[S1] The sample was irradiated by a continuous-wave (cw) laser of 532 nm at a power corresponding to the strong annihilation limit (see the main text), denoted $I_{\mathrm{UC}}^{\mathrm{Ex}}$. Under the same optical alignment, the reference was irradiated by a cw laser of 405 nm at a power of $I_{\mathrm{R}}^{\mathrm{Ex}}$, which was typically 0.5–2 mW. The optical paths of these two laser beams were aligned to be identical using irises and their spot diameter on the sample was set to 0.8 mm by adjusting the aperture of a mechanical iris placed just before the sample while monitoring the laser spot profile using a CCD laser beam profiler (Ophir-Spiricon, SP620). To obtain photoemission intensities from the sample and reference, denoted $I_{\mathrm{UC}}^{\mathrm{Em}}$ and $I_{\mathrm{R}}^{\mathrm{Em}}$, respectively, the measured photoemission spectra were corrected by the wavelength-dependent sensitivities of the system (i.e., for the monochromator grating and CCD; see the Experimental section in the main text) and then the spectra were integrated by the wavelength.

The general functional form used for the reference method is given by[S2,S3]

$$\Phi_{\mathrm{UC}} = \Phi_{\mathrm{R}} \left(\frac{1-10^{-A_{\mathrm{R}}}}{1-10^{-A_{\mathrm{UC}}}}\right) \left(\frac{I_{\mathrm{UC}}^{\mathrm{Em}}}{I_{\mathrm{R}}^{\mathrm{Em}}}\right) \left(\frac{I_{\mathrm{R}}^{\mathrm{Ex}}}{I_{\mathrm{UC}}^{\mathrm{Ex}}}\right) \left(\frac{h\nu_{\mathrm{UC}}}{h\nu_{\mathrm{R}}}\right) \left(\frac{n_{\mathrm{UC}}}{n_{\mathrm{R}}}\right)^{2}. \qquad \text{(S1)}$$

Here, A, $h\nu$, and n represent the absorbance, photon energy at the irradiation wavelength, and refractive index of the solvent, respectively. The subscripts "UC" and "R" indicate the UC sample and reference, respectively. In the second factor on the right hand side of eq. S1, one has to use $1-10^{-A}$, which represents the fraction of light absorbed or absorptance, instead of its approximated simplified form of "A" that is only valid when A is sufficiently smaller than 1.[S3] In the present samples, A at the excitation wavelength (532 nm) is above 0.1 (see Fig. 2b).

There is a point that should be noted regarding the form of eq. S1 in relation to the experimental conditions in this study. As described and discussed thoroughly in the Appendix of our previous paper[S4] and according to the basics provided in previous papers[S2,S5] and a textbook,[S6] the factor $(n_{\mathrm{UC}}/n_{\mathrm{R}})^2$ in eq. S1 was originally introduced to correct the situation in which a point photoemission source is located in a medium with half-infinite volume and the emission is taken out from it to the environment through the spatially extended planar interface (see, e.g., Fig. 2.44 of ref. S6). However, in our experimental situation, a small amount (~10 μL) of the sample liquid was sealed in a glass capillary tube with a cross section of 1 × 1 mm (see the Experimental section), which was held vertically in the air during the measurement. Thus, the rays of fluorescence emitted from the irradiated volume (laser beam diameter: 0.8 mm) of the sample, which has a small cross section (1 × 1 mm) on the horizontal plane, leaves the glass capillary radially and isotropically toward the environment, which is a quite different optical geometry from that originally considered for this correction.[S2,S5,S6] Thus, our experimental situation is not the same as that assumed for the correction factor $(n_{\mathrm{UC}}/n_{\mathrm{R}})^2$ introduced in the original papers.[S2,S5] This is at least considered to be true for the radial direction (i.e., for the horizontal plane), as has been confirmed by the ray-tracing simulation carried out in the Appendix of our previous paper.[S4] In contrast, for the axial direction of the glass capillary tube (i.e., for the vertical plane), the correction of $(n_{\mathrm{UC}}/n_{\mathrm{R}})$ may apply. Therefore, to correctly conform with the present experimental situation, eq. S1 should be rewritten as

$$\Phi_{\mathrm{UC}} = \Phi_{\mathrm{R}}\left(\frac{1-10^{-A_{\mathrm{R}}}}{1-10^{-A_{\mathrm{UC}}}}\right)\left(\frac{I_{\mathrm{UC}}^{\mathrm{Em}}}{I_{\mathrm{R}}^{\mathrm{Em}}}\right)\left(\frac{I_{\mathrm{R}}^{\mathrm{Ex}}}{I_{\mathrm{UC}}^{\mathrm{Ex}}}\right)\left(\frac{h\nu_{\mathrm{UC}}}{h\nu_{\mathrm{R}}}\right)\left(\frac{n_{\mathrm{UC}}}{n_{\mathrm{R}}}\right)^{i}, \qquad \text{(S1)'}$$

where i is a value somewhere between 0 and 1 (probably close to 1; however, its influence is eventually negligibly small as shown below).

To quantitatively evaluate this point, we carried out measurements of the refractive indexes of all the DESs used in this article and toluene at 450 nm, which is close to the wavelength of the fluorescence. All the measurements were conducted at 21 °C, which is the common temperature for all the experiments in this article. For the measurements, we used an Abbe refractometer (ATAGO, DR-M2), in which the temperature of the sample was controlled at 21.0±0.1 °C by a water-circulating loop. The light source was a broadband halogen lamp equipped in the system. Light of 450 nm was extracted using an optical band-pass filter (Edmund Optics, #65-140; full-width at half-maximum = 10 nm) inserted in the optical path after the light source. Table S3 summarizes the measured refractive indexes of all the solvents used in this article.

Table S3 Refractive indexes of the DESs used in this article measured at 450 nm.

Solvent	Refractive index[a]
N_{4444}Cl-$DA_{1:3}$ (used for sample #1)	1.4623
N_{4444}Cl-$DA_{1:2}$ (used for sample #2)	1.4679
N_{4444}Cl-$DA_{1:1.5}$ (used for sample #3)	1.4718
N_{4444}Cl-$DA_{1:1}$ (used for sample #4)	1.4770
N_{8888}Cl-$DA_{1:2}$ (used for sample #5)	1.4680
Toluene	1.5131

[a] Measured at 21.0±0.1 °C. The uncertainty caused from the visual reading in the measurement was within ±0.0002.

From the results, the term $(n_{\mathrm{UC}}/n_{\mathrm{R}})$ in the present case is ca. 0.97–0.98, which influences the magnitude of Φ_{UC} by only up to ca. 2.5/100 based on eq. S1′. This is one order of magnitude smaller than that of the error bar that we assumed for Φ_{UC} (±10%, which corresponds to the uncertainty of 20/100; see Fig. 3b). Because this magnitude is one order smaller than the experimental uncertainty, it does not influence the data. Therefore, all the values of Φ_{UC} in this article were calculated without explicitly including the refractive index term.

Determination of k_2: The second-order rate constant (k_2) in eq. 3 in the main text was obtained by analyzing the transient photoemission intensity decay curves of the UC fluorescence, which were experimentally acquired by the method described in the

Experimental section. For the measurements, a relatively high excitation pulse energy of 2 μJ/pulse (10 Hz) was used to achieve the dominance of the second-order decay in the early period of the decay (cf. Fig. S6 below), because such a condition was convenient for the analysis. The intensity decay curve was fitted by the theoretical decay function (eq. 5 of ref. S7). From the fitting, a dimensionless parameter Ω, which represents the ratio of the second-order decay over the first-order decay at time zero (t = 0),[S7] was obtained. The value of k_2 was calculated from the relationship[S7]

$$k_2 = \frac{k_\mathrm{T}\Omega}{[\mathrm{T}]_{t=0}}, \qquad \text{(S2)}$$

where k_T (= τ_T^{-1}) was determined in Fig. 5a and $[\mathrm{T}]_{t=0}$ is the initial concentration of the triplet DPA immediately after the completion of TET from PtOEP. $[\mathrm{T}]_{t=0}$ was readily calculated based on the standard method, i.e., by using the excitation pulse energy (2 μJ), the absorptance of the sample at the excitation wavelength, the photoirradiated diameter (0.8 mm) and length (1 mm) of the sample, the efficiency of TET (Φ_q in Fig. 4c), and Avogadro's number. It should be mentioned that the analytical framework used here as well as the consequences are essentially the same as those initially introduced by Weisman and Bachilo,[S8] although the appearance of the final form looked different. The validation of this analytical framework has been thoroughly carried out in our previous study[S7] and the related details including the mathematical derivation were described therein.

Determination of [$\mathrm{E_T}$]: The triplet emitter concentration under steady-state photoirradiation, denoted [$\mathrm{E_T}$], with the cw laser of 532 nm was determined by the following method. First, eq. 3 in the main text was rewritten for the steady-state conditions as

$$N_\mathrm{ex} = k_1[\mathrm{E_T}] + k_2[\mathrm{E_T}]^2, \qquad \text{(S3)}$$

and this was solved as[S9]

$$[\mathrm{E_T}] = \frac{-k_1 + \sqrt{{k_1}^2 + 4k_2N_\mathrm{ex}}}{2k_2}. \qquad \text{(S4)}$$

Here, N_ex is the rate of the formation of the triplet state in the emitters under the steady-state conditions. N_ex was calculated from the intensity of the laser light (532 nm), the sample absorptance at 532 nm, the efficiency of TET (Φ_q in Fig. 4c), and Avogadro's number. Because all the parameters on the right-hand side of eq. S4 are known, [$\mathrm{E_T}$] can be calculated using this equation.

Time-resolved intensity decay curves of the phosphorescence from PtOEP:

The measurement method was described in the Experimental section. The decays shown in Fig. S3a are slower than those shown in Fig. S3b because of the absence of the quencher DPA in the former.

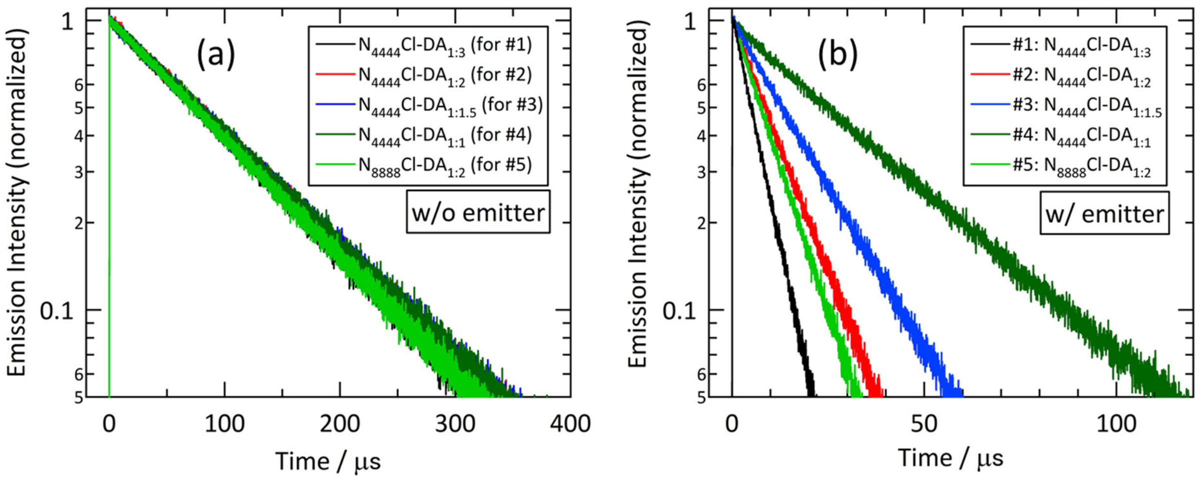

Fig. S3 Normalized time-resolved intensity decay curves of the phosphorescence from PtOEP (concentration: 5.5×10^{-5} M) monitored at 650 nm measured for (a) DESs that only contained PtOEP (i.e., no DPA) and (b) sample #1–#5 that contained DPA (3×10^{-3} M).

Fig. S3a revealed that the lifetime of the phosphorescence or the triplet lifetime of PtOEP in these DESs was almost invariant, as listed in Table S4.

Table S4 Phosphorescence lifetimes of PtOEP in the DESs used in this study, which were acquired by fitting the transient decay curves in Fig. S3a with a single exponential decay function

Type of DES[a]	**Phosphorescence lifetime [μs]** [b]
N$_{4444}$Cl-DA$_{1:3}$ (used for sample #1)	106
N$_{4444}$Cl-DA$_{1:2}$ (used for sample #2)	110
N$_{4444}$Cl-DA$_{1:1.5}$ (used for sample #3)	112
N$_{4444}$Cl-DA$_{1:1}$ (used for sample #4)	112
N$_{8888}$Cl-DA$_{1:2}$ (used for sample #5)	106

[a] See the main text for details of the notation. [b] Uncertainty of ±3% is considered to exist.

Stern–Volmer plots obtained from triplet quenching experiments:

Fig. S4 below shows some typical examples of the Stern–Volmer plots obtained from the results of the phosphorescence quenching experiments. From the slope of the plot, k_q (cf. Fig. 4a) was obtained.

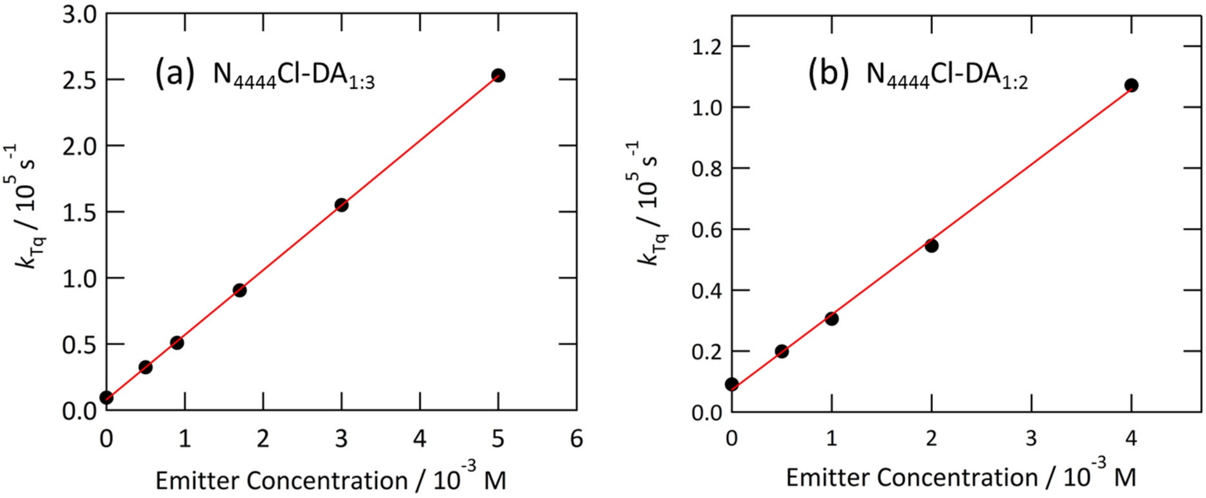

Fig. S4 Stern–Volmer plots obtained for (a) N_{4444}Cl-$DA_{1:3}$ and (b) N_{4444}Cl-$DA_{1:2}$. The vertical axis k_{Tq} is the decay time constant of the intensity of the phosphorescence from triplet PtOEP.

Time-resolved intensity decay curves of the UC fluorescence under weak pulsed excitation:

To determine the triplet lifetimes of DPA (τ_T) in sample #1–#5, they were irradiated by light pulses with relatively low energy (0.2 μJ/pulse) to attain conditions where the first-order decay dominates, as stated in the main text. The method of the lifetime experiment was described in the Experimental section. Under these conditions, transient intensity decay curves of the UC fluorescence nearly obeyed single-exponential decay. Fig. S5 shows the obtained intensity decay curves. These decay curves were fitted by the theoretical function (eq. 5 in ref. S7) that was also used to determine k_2. From this process, the value of τ_T for each sample was obtained.

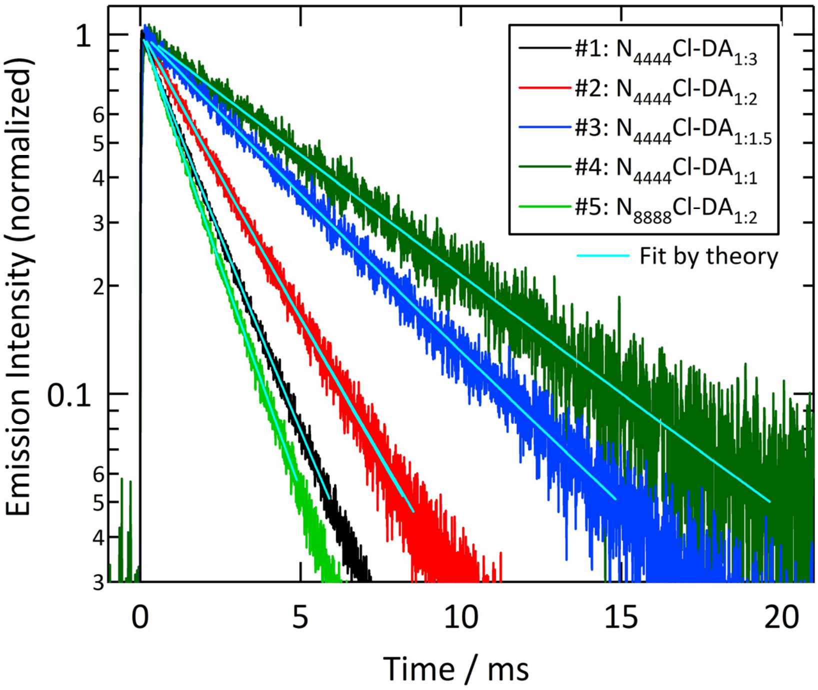

Fig. S5 Normalized transient intensity decay curves of the UC fluorescence from the samples after excitation with a pulse energy of 0.2 μJ. The light blue lines are the fits obtained using the theoretical decay function.

Time-resolved intensity decay curves of the UC fluorescence under strong pulsed excitation:

Fig. S6 depicts the time-resolved intensity decay curves of the UC fluorescence measured under strong pulsed-excitation conditions (pulse energy: 2 μJ/pulse), where the second-order decay dominates, along with the fits obtained by the theoretical function. The results look similar to those in Fig. S5 except that the decays are now apparently non-linear because of the much more remarkable second-order decay of the triplet states.

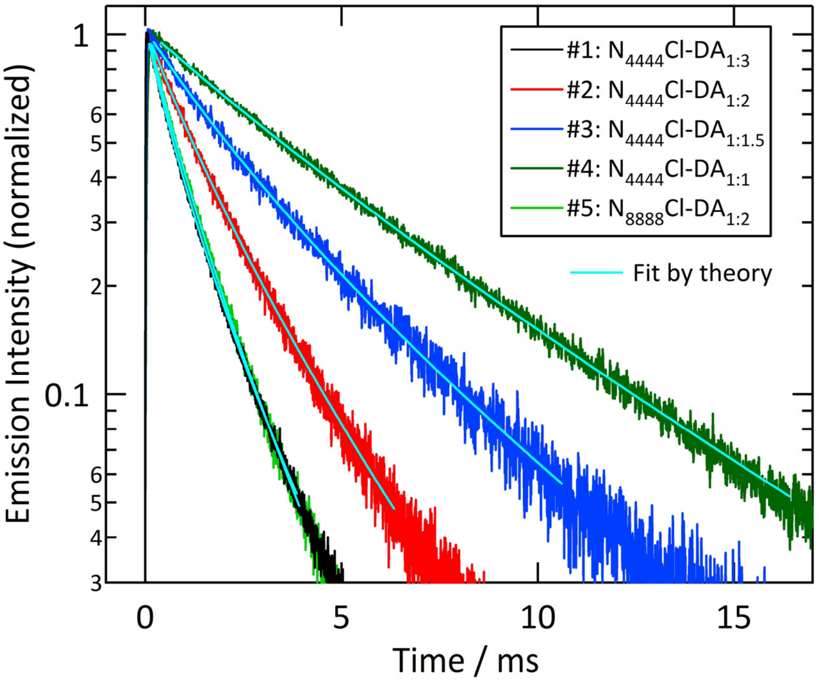

Fig. S6 Normalized transient intensity decay curves of the UC fluorescence from the samples after excitation with a pulse energy of 2 μJ. The light blue lines are the fits obtained using the theoretical decay function.

Further details of the equipment and analysis of the time-resolved fluorescence anisotropy decay measurements:

Microscopic viscosity felt by a solute in a solvent can be studied by several methods; one is investigation of the rotational relaxation time (also referred to as the “reorientation time” or “rotational correlation time”) denoted τ_{rot}. This characteristic time can be measured by time-resolved fluorescence anisotropy decay measurements.[S6,S10] In this article, the measurements were carried out based on the time-correlated single-photon counting (TC-SPC) technique. Specifically, τ_{rot} of DPA at 21 °C in each DES used in this study was measured using our custom-built TC-SPC system. Although the method of this experiment has already been described in the Experimental section of the main text, below we provide further information about the equipment and analysis.

Excitation light pulses: The light pulses used for sample excitation were of 405 nm and repeated at 8 MHz (pulse duration: ca. 200 fs). The pulses were generated by doubling the 810-nm light pulses that came out of a pulse picker (Spectra Physics, 3980), which was placed after a wavelength-tunable Ti:sapphire femtosecond laser oscillator (Spectra Physics, Tsunami 3941) operating at 80 MHz.

Measurement system: The experimental system for the measurements was designed and built by us and is schematically depicted below.

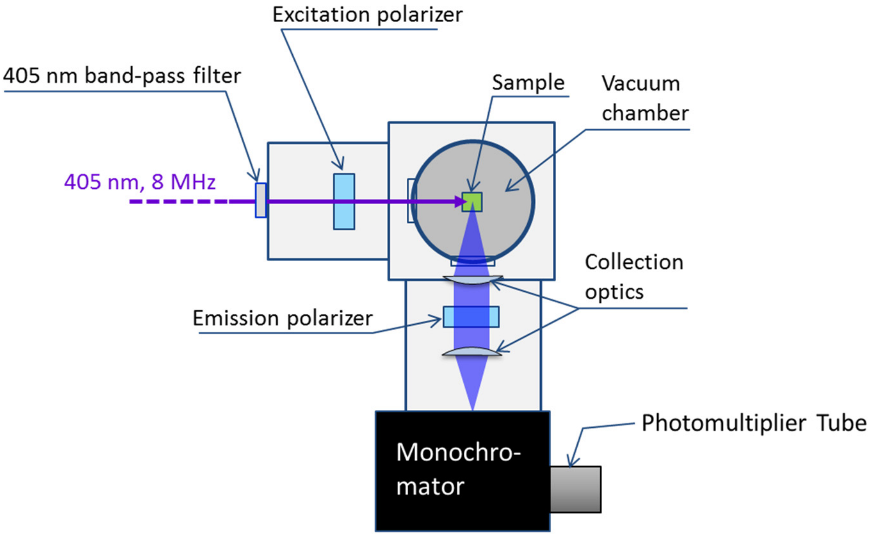

This system is based on the standard "L-format" measurement[S6] in which the directions of the photoexcitation and fluorescence collection are at right angles. As is usual,[S6] polarizers were placed before and after the sample. The system consisted of a vacuum chamber in which a temperature-controlled cuvette holder was placed, a pair of fluorescence collection optics, a monochromator, and a photomultiplier tube (Hamamatsu Photonics, R3809U-50). The electrical signal output from the photomultiplier tube was sent to a TC-SPC board (Becker & Hickl, SPC-130-EM) installed in a PC. The instrumental response function (IRF) was acquired by measurement of the light scattering from an aqueous suspension of fumed silica powder; the full width at half-maximum was ca. 42 ps.

Data analysis: The photoemission anisotropy at time *t*, denoted *r*(*t*), was calculated using the following relationship[S6]

$$r(t) = \frac{I_{VV}(t) - G \cdot I_{VH}(t)}{I_{VV}(t) + G \cdot 2I_{VH}(t)},$$

where the subscript "V" (vertical) and "H" (horizontal) represent the orientation of the polarizer with respect to the laboratory coordinate. For example, $I_{\mathrm{VV}}(t)$ represents the transient fluorescence intensity measured with both the excitation and emission polarizers positioned vertically, and $I_{\mathrm{VH}}(t)$ represents that measured with the excitation and emission polarizers set to vertical and horizontal orientations, respectively. "*G*" is the instrumental factor, which represents the ratio of the sensitivities of the detection system for vertically and horizontally polarized light at the emission wavelength, and was experimentally determined by[S6]

$$G = \frac{\int I_{HV}(t)dt}{\int I_{HH}(t)dt}.$$

For the present system, *G* was determined to be 1.20. To obtain *r*(*t*), first, the measured I_{VV} and I_{VH} signals were deconvoluted using the aforementioned IRF. The deconvolution was performed using the MATLAB® *deconvwnr* function with a noise-to-signal ratio (NSR) of 2. Then, the transient curve of *r*(*t*) was fitted by a double-exponential decay function, which physically corresponded to the anisotropic rotation of the non-spherical DPA molecule, expressed as

$$r(t) = A\exp\left(-\frac{t}{\tau_1}\right) + B\exp\left(-\frac{t}{\tau_2}\right),$$

where *A* and *B* are the coefficients and τ_1 and τ_2 are the decay time constants. Finally, $<\tau_{\mathrm{rot}}>$, which is the relaxation time averaged over the rotational axes, was calculated by the following relationship[S10]

$$\langle \tau_{\mathrm{rot}} \rangle = \frac{A}{A+B}\tau_1 + \frac{B}{A+B}\tau_2 \,.$$

Weight changes of the materials used in the DESs by drying treatment:

As described in the Experimental section of the main text, all the starting materials ($N_{4444}Cl$, $N_{8888}Cl$, and DA; see also Figs. 1b and 1c) used to prepare the DESs were dried prior to use. Fig. S7 shows the normalized time-dependent changes of their weights during drying. All of them displayed decreases in weight, which were ascribed to the removal of moisture. The weight decrease stopped after around 4–6 h for all the materials. Based on this, the time of 6 h was chosen for the drying treatment.

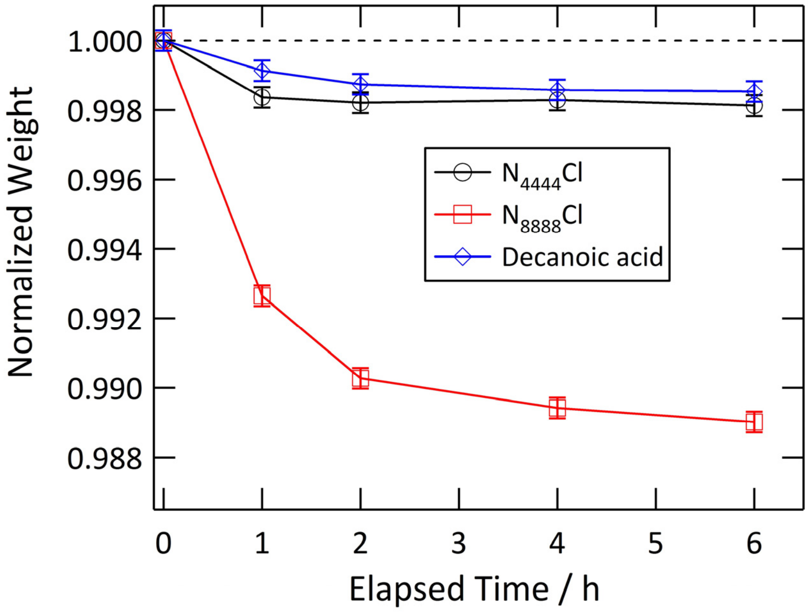

Fig. S7 Time-dependent changes in the weights of the materials during drying. The weights are normalized to the initial weights.

Effects of moisture absorption and nitrogen gas purging on measured viscosities:

As described in the Experimental section of the main text, during the viscosity measurements, nitrogen gas purging was carried out using our custom-built setup. A cylindrical plastic enclosure covered the entire sample section of the rheometer (Brookfield, R/S Plus) and dry nitrogen gas was continuously supplied into it. Fig. S8 below shows the effects of gas purging by comparing the changes in the measured viscosities with and without the purging. The horizontal axis represents the elapsed time, where the time zero is the point when the enclosure was removed and the purging was stopped. Each dot in this figure represents the value of the viscosity determined from each measurement that took about 2 min. The liquid measured in this figure was $N_{4444}Cl\text{-}DA_{1:2}$. The temperature during this experiment was controlled at 20 °C. When the sample section was purged with nitrogen (time < 0), the viscosity did not change with time. However, after the purging was stopped, the viscosity monotonically decreased, indicating that moisture adsorption had a remarkable influence on the viscosity of the DES. During this experiment, the relative humidity and temperature in the laboratory were 57% and 22 °C, respectively.

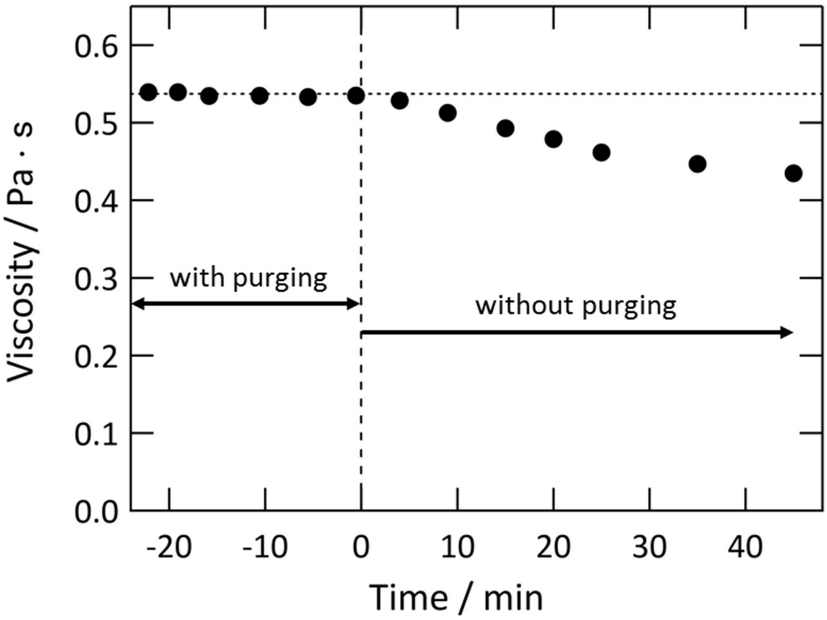

Fig. S8 Plot of the viscosity change of the DES $N_{4444}Cl\text{-}DA_{1:2}$ over time. For time < 0, nitrogen purging was carried out. At time = 0, the purging was stopped and the sample was exposed to the laboratory atmosphere. During the measurements, the temperature of the sample was controlled at 20 °C. The relative humidity and temperature in the laboratory during the measurements were 57% and 22 °C, respectively.

References

[S1] A. Demeter, *J. Phys. Chem. A*, 2014, **118**, 9985−9993.
[S2] J. N. Demas, G. A. Crosby, *J. Phys. Chem.*, 1971, **75**, 991−1024.
[S3] C. E. McCusker and F. N. Castellano, *Top. Curr. Chem.*, 2016, **374**, 19-1–19-25.
[S4] Y. Murakami, *Chem. Phys. Lett.*, 2011, **516**, 56–61.
[S5] E. H. Gilmore, G. E. Gibson, D. S. MoClure, *J. Chem. Phys.*, 1955, **23**, 399–399.
[S6] J. R. Lakowicz, *Principles of Fluorescence Spectroscopy, Third Edition*, Springer 2006.
[S7] Y. Murakami, H. Kikuchi and A. Kawai, *J. Phys. Chem. B*, 2013, **117**, 5180–5187.
[S8] S. M. Bachilo, R. B. Weisman, *J. Phys. Chem. A*, 2000, **104**, 7711–7714.
[S9] T. W. Schmidt, F. N. Castellano, *J. Phys. Chem. Lett.*, 2014, **5**, 4062–4072.
[S10] S. K. Das, M. Sarkar, *J. Phys. Chem. B*, 2012, **116**, 194–202.